

# Microwave absorption studies of polyaniline nanocomposites encapsulating gold nanoparticles on the surface of reduced graphene oxide in the presence of 2-naphthalene sulfonic acid

C. Basavaraja · Won Jung Kim · Dae Gun Kim ·  
Do Sung Huh

Received: 6 November 2011 / Revised: 9 January 2012 / Accepted: 12 January 2012 / Published online: 10 February 2012  
© Springer-Verlag 2012

**Abstract** Polyaniline nanocomposites containing gold nanoparticles (GNPs) attached to the surface of reduced graphene oxide (RGO) were chemically prepared using  $\beta$ -naphthalene sulfonic acid as a dopant. The synthesized composites were characterized using Fourier transform infrared spectroscopy and UV-vis spectroscopy, and their surface morphology and amended crystallinity were determined by scanning electron microscopy and X-ray diffraction, respectively. Further the elemental analysis was also performed to identify the synthesized polymer composites. Complex impedance measurements were performed on the composite samples in the form of films. Sheets prepared by conventional techniques were used to study the microwave absorption properties in the microwave range of 2–12 GHz, and the effects of sample thickness on the microwave absorption were investigated. Experimental results show that the electrical conductivity of the composites increases with increasing concentrations of added GNP-RGO without a percolation threshold.

**Keywords** Conducting polymer · Graphene oxide · Gold nanoparticles · Polymer-composites · Surface properties

## Introduction

Microwave-absorbing materials typically consist of shaped structures with properties that allow electromagnetic (EM) waves to penetrate into regions where electric and magnetic fields experience loss [1, 2]. For dielectric absorbers, loss is

primarily generated via the finite conductivity of the material. Incident EM waves impinging upon a conductive surface induce currents as the electric field interacts with mobile electrons within the material. Additional loss can also occur via molecular polarization phenomena, such as dipole rotation, space charge relaxation, and hopping of confined charges [3]. The electrical energy is dissipated as heat due to the resistance of the material. Conductive materials are important in various technologies, including stealth, electrostatic charge dissipation, and EM interference shielding [4, 5]. The design of microwave-absorbing materials requires control over several material properties, such as conductivity and complex permittivity. Such materials incorporate conductive additives or fillers into an insulating binder or matrix, where the matrix acts like a capacitor. The effectiveness of the absorber depends on the conductivity of the filler and the degree of its dispersion in the composite. Filler materials used in microwave absorbing composites include metals, such as iron or nickel, and carbon black or fibers [6].

Micro/nanostructured polyaniline (PANI) has received considerable attention because of its unique properties, including controllable chemical and electrical properties, simple preparation, low cost, and excellent environmental stability [7]. Such properties have led to the application of PANI in various micro/nanomaterials and devices [8]. The optical, microwave absorption, and magnetic functions of PANI micro/nanostructures have also attracted significant research interest because of their potential to meet the needs of a number of technological applications [9].

Polymer modification by surfactants is an attractive and interesting method for the preparation of polymer composites. Polymers have been widely studied both in solution and in the solid state because of their interesting physical properties, which include easy solubility, mesomorphic

C. Basavaraja · W. J. Kim · D. G. Kim · D. S. Huh (✉)  
Department of Chemistry and Institute of Basic Science,  
Inje University,  
Kimhae, Kyungnam 621-749, South Korea  
e-mail: chemhds@inje.ac.kr

behavior, nanostructured morphology, and reversible fusibility.  $\beta$ -naphthalene sulfonic acid (NSA), a well-known acid surfactant, forms colloidal particles and acts as a steric stabilizer because of its small size, thus it disperses evenly in aqueous media [10]. The anilinium-NSA complex can be obtained by mixing an emeraldine base of PANI with NSA, either mechanically or in solution. NSA in the solution state adsorbs most of the aniline monomers onto its complex network [11, 12]. The long aliphatic chains of NSA facilitate the process of mixing to yield the PANI-NSA complex, and the long hydrocarbon tail of the surfactant easily modifies the polymer-polymer interface in the complex.

Composites of organic/inorganic nanostructures have recently attracted significant attention due to their excellent physical, mechanical, and electrical properties, which include elevated conductivity, catalytic activity, gas sensitivity, and optoelectronic properties [13, 14]. In comparison with their bulk counterparts, one-dimensional nanostructures, such as wires, rods, belts, and tubes, have become the focus of intensive research because of their unique applications in mesoscopic physics and the fabrication of nanoscale devices [15, 16]. Gold nanoparticles (GNPs) have been widely studied as a component in polymer composites because of their unique, size-related electronic and optical properties [17]. GNPs dispersed into polymeric networks are currently used in sensors [18], catalytic purposes [19], conductive inks [20], and electron or energy storage [21].

Graphene and its derivatives have also attracted considerable attention in recent years because of their unique physical properties [22–24].

A potentially cost-effective method for mass-production of graphene-based devices is initiated by the production of chemically modified graphene, such as graphene oxide (GO), and then reduced for device applications. Large amount of GO can be easily produced by the chemical exfoliation of graphite through oxidation and the subsequent dispersion in water [25]. The basal plane and edges of GO are decorated with oxygen functional groups [26–28], making GO highly soluble in water. Single-layer GO sheets can be generated by simple sonication of hydrophilic graphite oxide in water. Considerable progress has also been made in the preparation of graphene oxide-polymer (GO-polymer) and reduced graphene oxide-polymer (RGO-polymer) composites, and significant enhancements in the mechanical and thermal properties of GO have been observed [29–32]. Thus, we have reported on the preparation and microwave absorption properties of PANI-gold nanoparticles-GO composites synthesized by *in situ* oxidation of aniline hydrochloride using hydrogen tetrachloroaurate as an oxidant [33]. However, the electrical conductivity of GO is low. The lower electrical conductivity of GO is due to the disruption of the  $sp^3$  bonded graphitic structure by the attachment of electronegative oxygen atoms [34]. GO can be

made highly conducting by exposing it to reducing agents such as hydrazine [35],  $NaBH_4$  [36]. The chemical reduction process of GO is usually regarded as the temperature-dependent structural transformation from the  $sp^3$  carbon-oxygen bonds to  $sp^2$  hybridized carbon bonds which leads to better conductivity.

In the present paper, we report *in situ* chemical oxidation of aniline hydrochloride in the presence of different weight percentages of GNPs dispersed on RGO (GNP-RGO) using APS as an oxidant in the presence of naphthalene sulfonic acid. The synthesized nanocomposites were characterized by Fourier transform infrared spectroscopy (FTIR) and UV-vis spectroscopy, and their morphology was investigated by scanning electron microscopy (SEM) and transmission electron microscopy (TEM). Crystallinity was studied through X-ray diffraction (XRD) analysis. Measurements of the DC electrical conductivity of the nanocomposites at room temperature, as well as determination of changes in microwave absorption in the range of (2 to 12) GHz with increasing GNP-RGO loading, were performed on composite samples in the form of films.

## Experimental part

### Materials

Sodium borohydride ( $NaBH_4$ ), gold (III) chloride trihydrate ( $HAuCl_4 \cdot 3H_2O$ , 99.0%), and NSA ( $C_{10}H_8O_3S \cdot H_2O$ ) were purchased from TCI Fine Chemicals. *N*-Methyl-2-pyrrolidone (NMP) was obtained from Junsei Chemical Co. Graphite (synthetic powder <20  $\mu m$ ), all other reagents was purchased from Sigma-Aldrich and used as-received without further purification. For all practical purposes, double-distilled (DI) water was used.

### Preparation of reduced graphene oxide (RGO)

GO was prepared from purified natural graphite according to a modified Hummers method [37, 38]. Approximately 1–2 g graphite powder, 0.75–1 g  $NaNO_3$ , and 3–4 g  $KMnO_4$  were dissolved in 75–100 mL concentrated  $H_2SO_4$ . The solution was vigorously stirred for 7 h at room temperature. Approximately 250 mL of 5% aqueous  $H_2SO_4$  solution was then added to the mixture, which was kept at 98 °C for 2 h. The temperature was reduced to room temperature, and  $H_2O_2$  (30%, 10 mL) was slowly added. The reaction mixture was further stirred for 2 h and centrifuged to collect the bottom layer, which was sequentially washed with 5%  $H_2SO_4/0.5\%$   $H_2O_2$  (15 times) and 5% HCl solution (5 times), and then repeatedly washed with distilled water until the pH of the supernate was neutral. Finally, the material was dried and a loose brown powder was obtained.

RGO was prepared by chemical reduction of GO with  $\text{NaBH}_4$ . 0.3 g of GO was dispersed in 50 mL of DI water. Approximately 0.5 g  $\text{NaBH}_4$  was then added to the mixture, and the mixture was heated at 100 °C for 24 h. After the reaction was completed, the solid RGO was centrifuged and repeatedly washed with DI water. The final product was dried overnight in a vacuum oven at 80 °C.

#### Preparation of gold nanoparticles dispersed on RGO (GNP-RGO)

To prepare GNP-RGO, 0.1 g RGO was dispersed in 35 mL of DI water. Then, 0.4 mL of chloroauric acid (0.02 M) was added to the RGO suspension with stirring. The mixture was kept at room temperature for 3 h with constant stirring. After repeated washing with DI water, the product was dried at 60 °C for 24 h. The sample will be abbreviated as GRG.

#### Preparation of polyaniline–naphthalene sulfonic acid (PANI-NSA) polymers

PANI-NSA (PANS) was obtained by the polymerization of anilinium chloride in an aqueous medium with 0.5 M aniline hydrochloride in the presence of 1.5 M NSA using 0.1 M APS as an oxidant. Initially, 1.5 M NSA was placed together with aniline hydrochloride and the mixture was sonicated for about 20 min. Later the beaker containing the mixture was cooled to (0 to 5) °C, after which 0.1 M APS solution was slowly added to the mixture for about 30 min. Next, the reaction mixture was cooled in a refrigerator for about (4 to 5) h without sonication and then brought to room temperature. The precipitated PANS polymer powder was recovered by vacuum filtration and washed thoroughly with deionized water and acetone. Finally, the resulting powder was dried in a vacuum oven for 24 h to achieve a constant weight.

#### Preparation of the polyaniline–naphthalene sulfonic acid/ GNP-RGO (PANS/GRG) nanocomposites

PANS/GRG composites were prepared with varying amounts (wt %) of GNP-RGO (GRG) (0.1, 0.3, and 0.6 g). During the synthesis of the composites, the specific amounts of GRG were initially dispersed in aqueous medium. NSA solution was then added to the GRG dispersion, and the mixture was sonicated for about 30 min. Once a uniform dispersion of GRG and NSA was obtained, a known amount of aniline hydrochloride solution was added to the reaction mixture with continuous sonication. The sonication of the mixture was performed for another 30 min. Later, the beaker containing the mixture was cooled to (0 to 5) °C. APS solution was slowly added to this mixture for about 30 min, and the reaction mixture was cooled in a refrigerator for about (4 to 5) h without

sonication. Afterwards, the mixture was brought to room temperature. The precipitated PANS/GRG composite polymer powder was recovered by vacuum filtration and washed thoroughly with deionized water and acetone. Finally, the resulting powder was dried in a vacuum oven for 24 h to achieve a constant weight [39–41]. PANS/GRG nanocomposites with 0.1, 0.3, and 0.6 g of GRG will be denoted as PANS/GRG-1, PANS/GRG-3, and PANS/GRG-6, respectively for simplification.

#### Elemental analysis (EA)

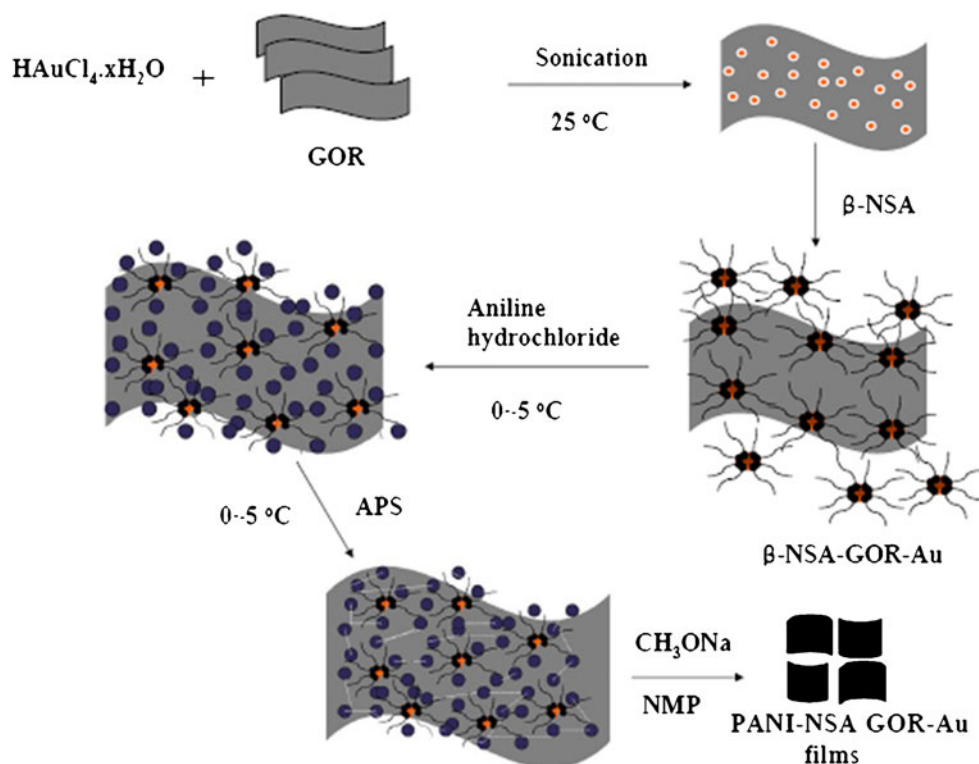
Elemental analysis for C, O, N, S, Au of the PANS, GRG, and PANS/GRG powder samples was carried out with a X-ray photoelectron Spectrometer (VG Scientifics, ESCALAB 250 XPS Spectrometer) at  $1 \times 10^{-10}$  torr using a  $\mu$ -metal chamber. Monochromated Al-K $\alpha$  ray was used as the energy source.

## Results and discussion

In our earlier research [33] we have used  $\text{HAuCl}_4$  as an oxidant in the polymerization of aniline hydrochloride in the presence of GO. During the present research we have slightly modified the process of method of polymerization to obtain PANS/GRG composites. In this study we have synthesized gold nanoparticle-reduced graphene oxide particles and are incorporated in the polymerization process of aniline hydrochloride in the presence of NSA. We have used NSA since it can wrap or en-capsule the spherical shaped GNP to the surface of RGO. So that the aniline hydrochloride molecules can be attached to the tails of NSA, and the polymerization for the polyaniline-gold/graphene oxide composite was possible. Figure 1 shows the schematic diagram for the formation of PANS/GRG composites. After the addition of NSA to the aqueous solution containing GRG, a uniform solution forms, which appears to be some kind of complex. To determine whether or not a complex forms between GNR and NSA, part of the solution was pipetted out and centrifuged before the addition of aniline hydrochloride. The powder sample was analyzed by electron microscopy. Figure 2a and b show the SEM and TEM image of GRG powder samples. The images show that GNPs attached to the surface of RGO. And the change in morphology after the addition of NSA to GRG is given in the SEM and TEM image as shown in Fig. 2c and d, respectively. The images of Fig. 2c and d suggest the formation of NSA/GRG complex structure.

After obtaining the NSA/GRG complex, aniline hydrochloride was added and the mixture was further sonicated for 10 min. Upon obtaining a uniform mixture, the solution was cooled and the temperature was brought to (0 to 5) °C.

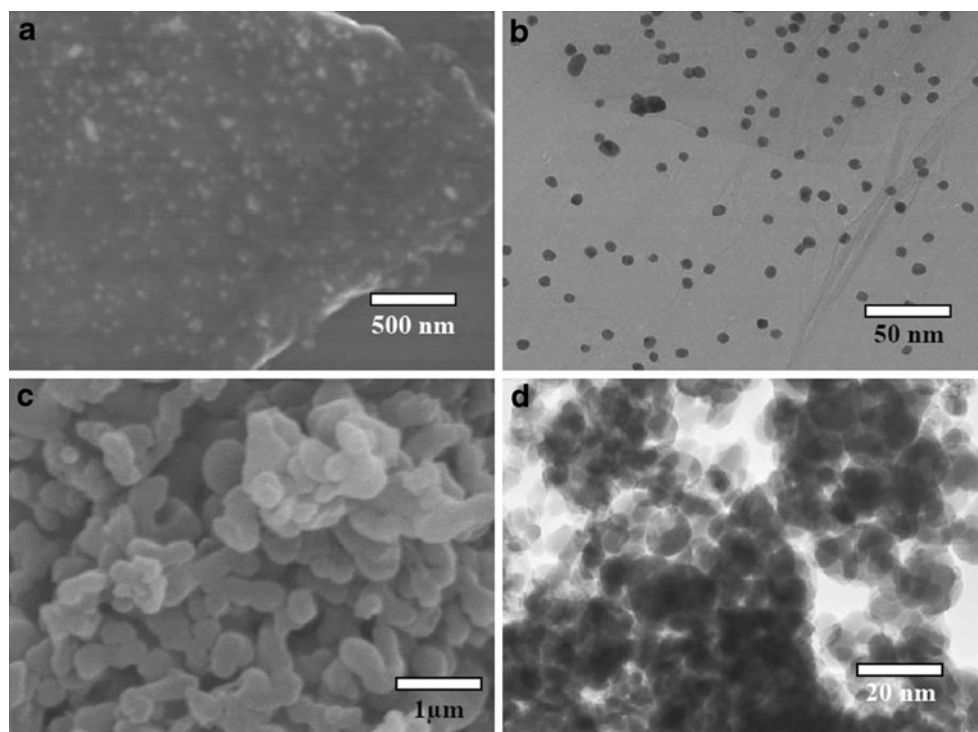
**Fig. 1** Schematic diagram showing the process for the formation of PANI-NSA/GNP-RGO (PANS/RGO) composite thin films



APS was slowly added to this solution, and the beaker was refrigerated in the temperature range of  $0\text{-}5\text{ }^\circ\text{C}$  for about (4 to 5) h to obtain PANI-NSA/GRG (PANS/GRG) composites. NSA acts as a soft-template during the polymerization process. Micelles composed by NSA can serve as soft-

templates due to the presence of  $-\text{SHO}_3$  groups in the structure of the surfactant. Polymerization takes place at the water/micelle interface due to hydrophilic APS, and the growth of the nanotubes or nanofibers is controlled by a polymerization and elongation process [43].

**Fig. 2** (a) SEM image of GNP-RGO (GRG) powder samples, (b) TEM image of GNP-RGO (GRG) powder samples, (c) the SEM image showing the change in morphology after the addition of NSA to GRG, and (d) TEM image of NSA/GRG





Characterization, surface morphology, and diffraction studies of PANS and PANS/GRG nanocomposites

Figure 3 shows the FTIR spectra of (a) GRG and NSA-GRG complex, (b) PANS, PANS/GRG-3, and PANS/GRG-6. The GRG shows peaks corresponds to both RGO and GNP particles. The GRG shows peaks at 3468, 2923, 2855, and 1655  $\text{cm}^{-1}$  corresponds to RGO of O-H, C-H, and C = C respectively. And the spectra also indicate the GNPs transmittance peaks at around 1390, 1635, and 1712  $\text{cm}^{-1}$ . A wide absorption bands observed at about 1606 and 1622  $\text{cm}^{-1}$  are attributed to the stretching vibration of -C = C- [44]. In addition, the weak absorption bands observed in the range of 1700–1800  $\text{cm}^{-1}$  can be attributed to the stretching vibration of -C = O [45]. The transmittance peak at 3440  $\text{cm}^{-1}$  was caused by traces of water in the nanoparticle sample. Further the NSA-GRG complex shows all

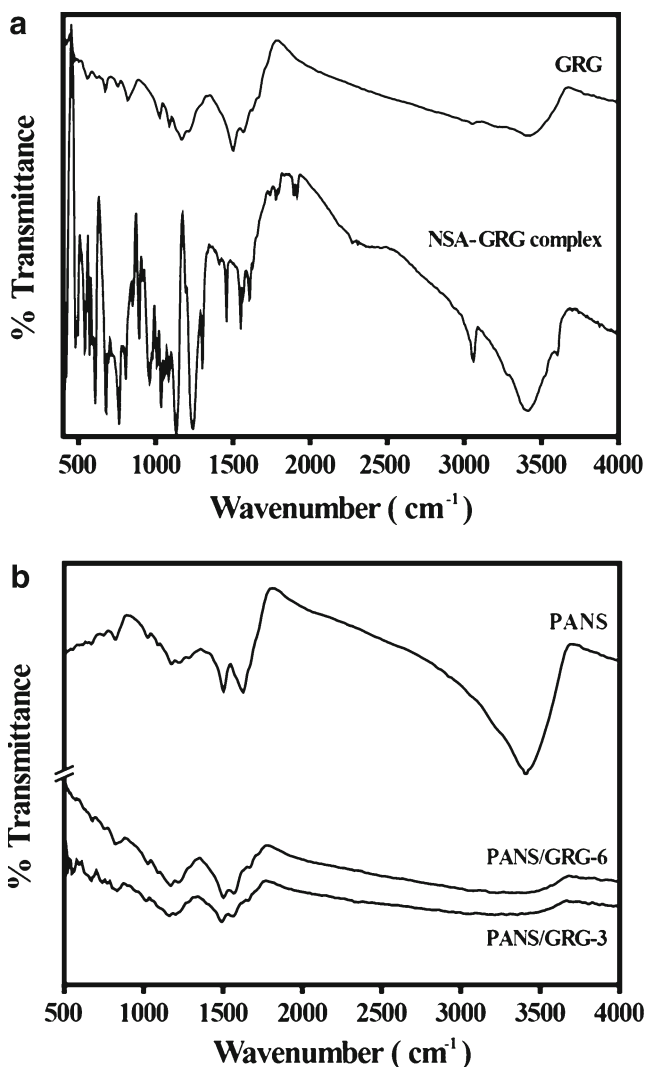


**Fig. 3** FTIR spectra of (a) GRG and NSA-GRG complex, (b) PANI-NSA (PANS), PANS/GRG-3, and PANS/GRG-6

the transmittance peaks present in GRG. The new peaks at 1026 and 676  $\text{cm}^{-1}$  can be ascribed to the absorption of  $-\text{SO}_3^-$  of NSA which also appears in PANS and PANS/GRG composites [42]. The appearance of both GRG peaks and  $-\text{SO}_3^-$  suggests the formation of NSA-GRG complex. PANS shows strong peaks at 3224  $\text{cm}^{-1}$ , which are attributed to N-H stretching, (1627 and 1496)  $\text{cm}^{-1}$ , which are attributed to benzenoid and quinoid rings, respectively, 1296  $\text{cm}^{-1}$ , which are attributed to C-N stretching of the secondary aromatic amine, 1141  $\text{cm}^{-1}$ , which is attributed to C = N stretching, and 805  $\text{cm}^{-1}$ , which is attributed to 1,4-substituted phenyl ring stretching [46–48]. These peaks are similar to the emeraldine salt form of PANI, but they are red-shifted by a factor of about (10 to 15)  $\text{cm}^{-1}$  compared with PANI, which implies the formation of PANI-NSA. Compared with RGO, the bands of GRG are blue-shifted, which may be due to the presence of gold nano particles in the RGO network [44, 45]. The weak bands at (3423 and 1397)  $\text{cm}^{-1}$  are attributed to deformations of the -OH and -COOH groups, respectively. The band situated at 1054  $\text{cm}^{-1}$  is assigned to C-O stretching vibrations. The stretching vibration of carbonyl or carboxyl groups is observed at 1724  $\text{cm}^{-1}$ . The bands at (1211 and 1608)  $\text{cm}^{-1}$  are attributed to C-OH stretching and C = C stretching of the aromatic ring, respectively. The FTIR bands for GRG remain almost identical in the spectra for PANS/GRG-3 and PANS/GRG-6. Careful observations, however, show the following: The quinoid ring remains unchanged in both nanocomposites, but the benzenoid ring is shifted to (1635 and 1543)  $\text{cm}^{-1}$  in PANS/GRG-3 and PANS/GRG-6, respectively. Furthermore, the 1,4-substituted phenyl ring stretching is observed at 817  $\text{cm}^{-1}$  in both PANS/GRG-3 and PANS/GRG-6. The band for C = N stretching remains unchanged in both nanocomposites.

To obtain the UV-vis spectra of PANS and PANS/GRG composites, a 2 mg/mL solution of each nanocomposite was prepared in NMP. The solution was sonicated for about 10 min and a uniform color of the solution was ensured before measurement. Figure 4 shows the UV-vis spectra of PANS, PANS/GRG-3, and PANS/GRG-6. PANS shows two broad absorption bands, one at around 290 nm and the other at 630–650 nm. The first one is due to  $\pi \rightarrow \pi^*$  transition of the benzoid and quinoid structure, and the second one is due to the transition of exciton in the PANI backbone [49]. The spectra of PANS/GRG-3 indicate three absorption bands, one of which is nearly a sharp peak at around 300 nm is due to  $\pi \rightarrow \pi^*$  is combined with RGO peak, the second absorption peak at around (480 to 550) nm in PANS/GRG-3 is due to the presence of GNP in the composite [50], and the third band at around 650 nm due to the transition of exciton in the PANI backbone [51]. The absorption spectra of PANS/GRG-6 are similar to those of PANS/GRG-3, but the second band near 650 nm is slightly broader and the third is slightly sharper. The presence of the three bands

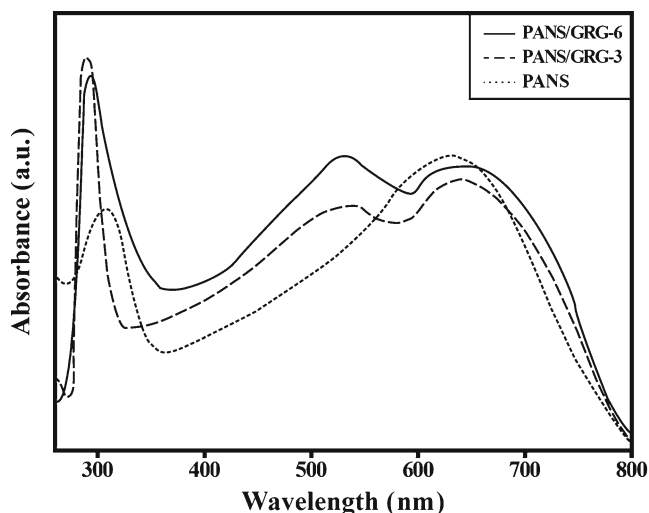


**Fig. 4** UV-vis spectra of PANS and PANS/GRG composites

suggests the formation of PANS/GRG composites. A rather broad absorption band-shift to higher wavelengths is verified for PANS/GRG-6, suggesting the presence of particle aggregates. Both FTIR and UV-vis spectral results not only demonstrate the presence of PANS and GRG in the PANS/GRG composites, but also suggest the combination of these two components by showing some kind of interaction via doping/incorporation.

Figure 5 shows SEM images of sample films for PANS (a, b), PANS/GRG-1 (c, d), PANS/GRG-3 (e, f), and PANS/GRG-6 (g, h) composites. The SEM image of PANS obtained at lower magnification (Fig. 5a) shows the formation of like a hard and rigid surface, while the high magnified image (Fig. 5b) indicates the appearance of lump-like structures. PANS can thus be suggested to form a uniform, rigid morphology. At a lower magnification (Fig. 5c), the surface SEM image of PANS/GRG-1 shows a structure that is almost similar to PANS, while the higher magnification image (Fig. 5d) shows spherical particles attached to lump-like structures. The particle size of the spherical particles is around (5 to 10) nm, whereas that of the lump-like structures is around 1  $\mu\text{m}$ .

Contrary to PANS/GRG-1, the image of PANS/GRG-3 shows scalar or flake-like surfaces (which are not clearly visible but were considered scalar) over lump-like structures with spherical particles attached at lower magnification (Fig. 5e). In comparison, the image obtained at higher magnification shows lump-like structures containing spherical particles (Fig. 5f). The particle size of the lumpy and spherical particles appears to be more or less the same as described above for PANS/GRG-1. From the images of PANS/GRG-6 at both lower and higher magnifications, spherical particles with sizes greater than those in PANS/GRG-1, nearly (20 to 25) nm, are found (Fig. 5g and 5h). The lumps appear smaller but are scattered here and there on

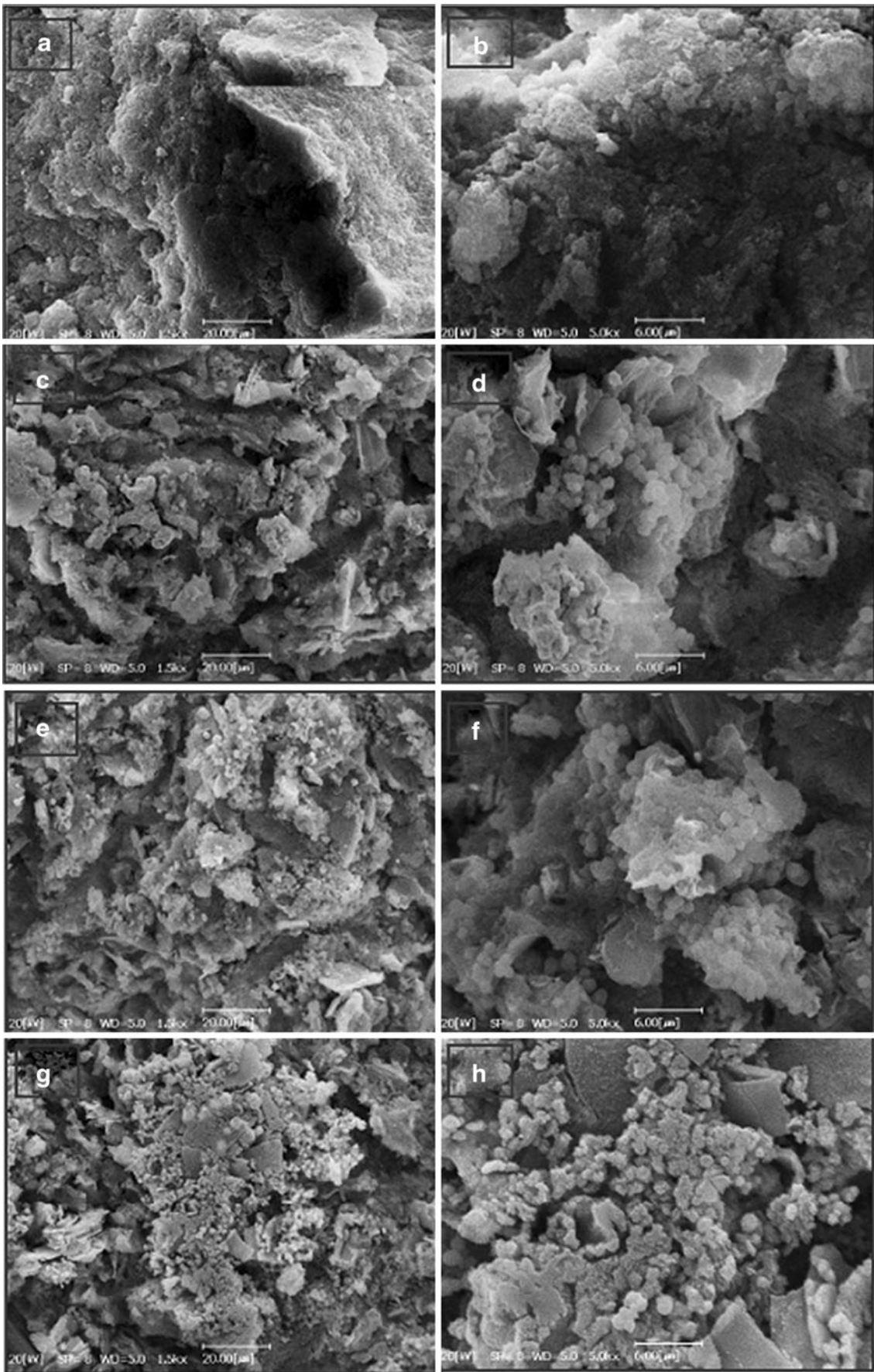
**Fig. 5** SEM images of sample films of (a, b) PANS, (c, d) PANS/GRG-1, (e, f) PANS/GRG-3, and (g, h) PANS/GRG-6 composites obtained at different magnification

the surface of the nanocomposite; the lumps are approximately 500 nm in size. The formation of PANS/GRG-6 suggests a possible reaction scheme, which is described in Fig. 1, as well as by the SEM and TEM images provided in Fig. 2. Figures 1 and 2 show that the addition of aniline hydrochloride may attach to the complex structure formed by the GNP-RGO-NSA particles because NSA possesses fibrillar structures, which allow the aniline hydrochloride to attach to it. Thus, the complex structure is formed. After the addition of APS, the aniline hydrochloride polymerizes to form PANS/GRG composites. From the RGO surface, a flake could appear over which the GNP particles might embed within PANS particles that attached to the RGO flakes.

Figure 6a shows the XRD pattern of GRG indicating the major Bragg reflection peaks at  $2\theta$  of  $38^\circ$ ,  $42^\circ$ ,  $64^\circ$ , and  $78^\circ$ , which are considered to be the (111), (200), (220), and (311), respectively, as the face-centered cubic structure of the GNPs [51, 52]. And Fig. 6b show the XRD patterns for PANS, PANS/GRG-1, PANS/GRG-3, and PANS/GRG-6. The XRD pattern of PANS shows two broad peaks centered at  $2\theta$  of  $20^\circ$  and  $25^\circ$ , which are assigned to planes perpendicular and parallel to the polymer chain, respectively [53]. The XRD peaks of PANS/GRG-1, PANS/GRG-3, and PANS/GRG-6 show similar patterns with those of GRG. The peak centered at  $2\theta$  of  $20^\circ$  and  $25^\circ$ , which are ascribed to the periodicity of the PANI chain in PANS [10] diminishes in PANS/GRG-1 and completely disappears in PANS/GRG-3 and PANS/GRG-6; its disappearance may be due to the decrease in the amorphous nature of PANI in both PANS/GRG-3 and PANS/GRG-6. The diffraction patterns of the PANS/GRG composites combine the diffraction peaks from both GRG and PAS, further proving the existence of GRG in the composites.

#### Elemental analysis of PANS, GRG, and PANS/GRG powder samples

Table 1 shows the result of elemental analysis for C, N, S, O, Au in the PANS, GRG, and PANS/GRG powder samples obtained by XPS. By the data, C, N, S, and O are all existent in the PANS polymer, which reveals that PANI-NSA (PANS) was obtained by the polymerization of anilinium chloride in an aqueous medium with aniline hydrochloride in the presence of NSA using APS as an oxidant. The higher percentage of O may be due to the doped NSA. The existence of C and Au as a higher percentage in the GRG sample was originated by the formation of a composite by graphine and GNP. The composition of N and O in GNP can be attributable to the oxidation and reduction process of





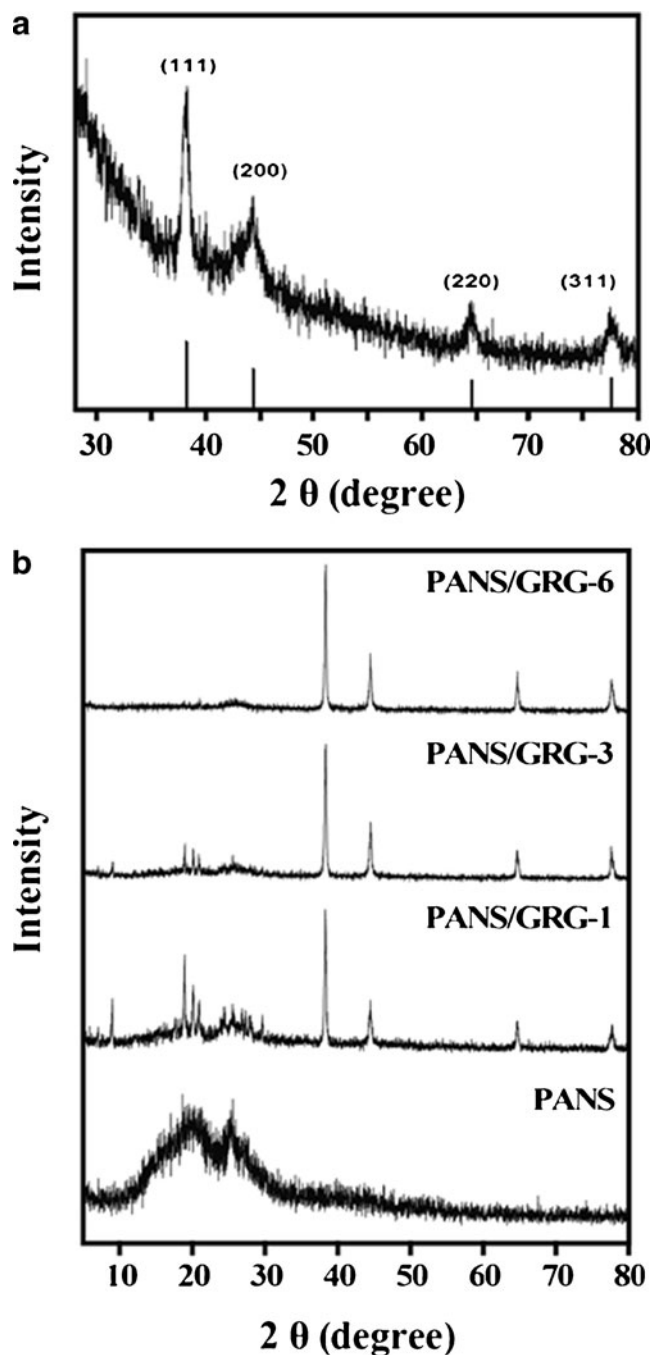


**Fig. 6** (a) XRD patterns of GRG, (b) XRD patterns of PANS, PANS/GRG-1, PANS/GRG-3, and PANS/GRG-6

graphene for RGO. The elemental analysis data also indicates that the percentage of C and Au increases by increasing the concentration of GRG in the PANS/GRG composites while the percentage of N and S decreases. The increase in the percentages of C is due to the additional carbon present in RGO. Therefore the increase of GRG has resulted in the increase of carbon percentage in the composites. Also the elemental analysis data indicate that the presence of oxygen in the composite decreases by increasing the concentration

**Table 1** Elemental analysis data of the PANS, GRG, and PANS/GRG composites

	Atomic percentage (%)				
	C	N	S	O	Au
PANS	64.06	7.21	7.08	13.15	
GRG	68.12	3.05	0.39	11.70	15.12
PANS/GRG-1	48.51	5.80	5.13	24.54	10.36
PANS/GRG-3	50.65	5.47	4.43	19.13	11.47
PANS/GRG-6	54.51	4.74	4.13	17.46	13.12

of GRG as can be observed in Table 1. The decrease in oxygen percentage is due to partial oxidation of the PANI chains in the formation of PANS/GRG composite. As the

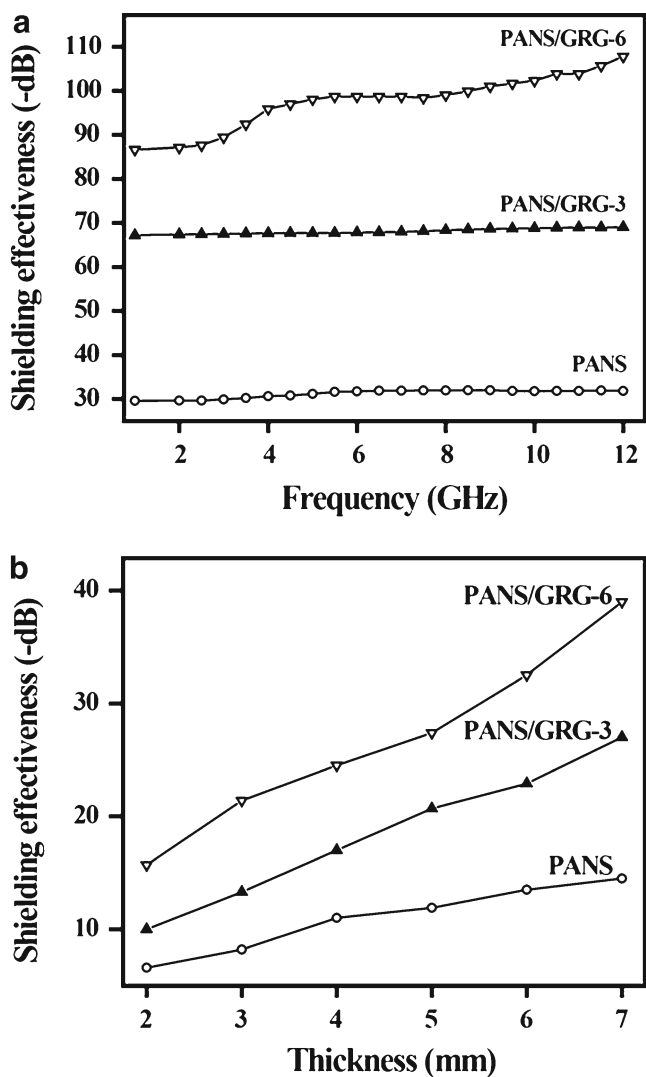


**Fig. 7** EMI radar cross section measurements of PANS and PANS/GRG composites, (a) as a function of frequency measured in the range of 1–12 GHz range, and (b) as a function of thickness (mm) measured in the frequency of 5.0 GHz



reaction scheme from the Fig. 1 we can suggest the involvement in oxygen during the formation of PANS/GRG composites.

#### Microwave absorption studies of PANS and PANS/GRG nanocomposites

The obtained conductivities of PANS, PANS/GRG-3, and PANS/GRG-6 were approximately  $(5.85 \times 10^{-4}, 3.29, \text{ and } 8.65) \text{ S/cm}$ , respectively; these values were obtained from composites in the form of pellets at room temperature as described in our earlier research [54]. The enhanced electrical conductivity of PANS and its nanocomposites indicates that the corresponding composites would show interesting microwave absorption behaviors. Figure 7 shows the electromagnetic wave interference (EMI) radar cross section (RCS) measurements of PANS and the PANS/GRG nanocomposites (a) as a function of frequency measured in the range of 1–12 GHz range, and (b) as a function of thickness (mm) measured in the frequency of 5.0 GHz. At an initial frequency of 1 GHz, the RCS values for PANS, PANS/GRG-3, and PANS/GRG-6 are 30, 67, and 87 dB, respectively, while those values at a higher frequency of 12 GHz are 32, 69, and 108 dB, respectively. The figure also shows that the RCS value of PANS and PANS/GRG-3 remains more or less same (or shows a small increase even with increasing weight percentages of GRG).

Figure 7b shows the EMI-RCS values as a function of thickness at a frequency of 5.0 GHz. In all composites, an increase in thickness resulted in an increase in RCS value. The enhanced microwave absorption of PANS/GRG-3 and PANS/GRG-6 compared with PANS. The EMI-RCS values in the composites may be due to the adhesion GRG, which supports the formation of PANS/GRG composites. The EMI-RCS values obtained from the PANS/GRG composites are higher compared with the values obtained in the previous studies in the literature [55–57]. However the EMI-RCS values of PANS/GRG composites are slightly lower as compared to the values reported by us in earlier studies for the PANI-GNP-GO composites [33].

The difference of EMI-RCS values between PANI-GNP-GO and PANS/GRG composites is not so significant. Based on these observations we can suggest that the preparation of PANS/GRG composites is rather cost-effective for interdisciplinary applications. The use of NSA can support in enhancing the interaction between PANI, GNP and RGO for the PANS/GRG composites.

#### Conclusion

New PANI composites were synthesized in the presence of different weight percentages of GNPs dispersed on RGO

using NSA as a dopant and characterized. These novel composites presented some interaction between PANI-NSA (PANS, organic part) and GNP-RGO (GRG, inorganic part) by mostly of the covalent type. Surface morphology data also suggest the formation of PANS/GRG composites. Furthermore, room temperature conductivity and EMI-RCS value were observed, and both values of the composites were increased with the increase of GRG percentage. The PANS/GRG composites studied in this paper may find future uses in various electrical applications where EMI shielding is considered to be important.

**Acknowledgment** This work was supported by the 2012 Inje University Research Grant.

#### References

- Zhang X, Sanjeev KM (2006) *Chem Commun*: 2477–2479
- Baibarac M, Gomez-Romero P (2006) *J Nanosci Nanotechnol* 6:1–14
- Geetha S, Sathesh Kumar KK, Chepuri RKR, Vijayan M, Trivedi DC (2009) *J Appl Polym Sci* 112:2073–2086
- Liu Z, Bai G, Huang Y, Li F, Ma Y, Guo T, He X, Lin X, Gao H, Chen Y (2007) *J Phys Chem C* 111:13696–13700
- Annadurai P, Mallick AK, Tripathy DK (2002) *J Appl Polym Sci* 83:145–150
- Makeiff DA, Huber T (2006) *Synth Met* 156(7–8):495–505
- MacDiarmid AG (2001) *Angew Chem Int Ed* 40:2581–2590
- Ramanathan K, Bangar MA, Yun M, Chen W, Myung NV, Mulchandani A (2005) *J Am Chem Soc* 127:496–497
- Goncharov A, Zhukov AA, Bartlett PN, Ghanem MA, Boardman R, Fangohr H, de Groot PAJ (2005) *J Magn Magn Mater* 286:1–4
- Shen Y, Wan M (1999) *J Polym Sci A Polym Chem* 37:151–157
- Jie H, Wan M (1999) *J Polym Sci A Polym Chem* 37:1443–1449
- Wei Z, Zhang Z, Wan M (2002) *Langmuir* 18:917–921
- Li F, Chai J, Yang H, Han D, Niu L (2010) *Talanta* 81:1063–1068
- Li D, Kaner RB (2008) *Science* 320:1170–1171
- Zhang K, Zhang LL, Zhao XS, Wu J (2011) *Chem Mater* 22(4):1392–1401
- Goswami S, Maiti UN, Maiti S, Nandy S, Mitra MK, Chattopadhyay KK (2011) *Carbon* 49:2245–2252
- Lebedeva OV, Kim BS, Grohn F, Vinogradova OI (2007) *Polymer* 48:5024–5029
- Olowu RA, Arotiba O, Mailu SN, Waryo TT, Baker P, Lwuoha E (2003) *Sensors* 19:7754–7758
- Zhao M, Crooks RM (1999) *Chem Mater* 11:3379–3385
- Grohn F, Bauer BJ, Akpalu YA, Jackson CL, Amis EJ (2000) *Macromolecules* 33:6042–6050
- Pudas M, Hagberg J, Leppavuori S (2004) *Prog Org Coat* 49:324–335
- Geim AK, Novoselov KS (2007) *Nat Mater* 6:183–191
- Ruoff R (2008) *Nat Nanotechnol* 3:10–11
- Hao Q, Wang H, Yang X, Lu L, Wang X (2011) *Nano Res* 4(4):323–333
- Ruoff RS (2008) *Nat. Nanotechnol* 3:10–11
- Cai W, Piner RD, Stadermann FJ, Park S, Shaibat MA (2008) *Science* 321:1815–1817
- Lerf A, He HY, Forster M, Klinowski J (1998) *J Phys Chem B* 102:4477–4482
- He HY, Klinowski J, Forster M, Lerf A (1998) *Chem Phys Lett* 287:53–56

29. Park JS, Cho SM, Kim WJ, Park J, Yoo PJ (2011) *ACS Appl Mater Interfaces* 3:360–368
30. Salavagione HJ, Gomez MA, Matinez G (2009) *Macromolecules* 42:6331–6334
31. Li D, Huang JX, Kaner RB (2009) *Acc Chem Res* 42:135–145
32. Wu Q, Xu YX, Yao ZY, Liu AR, Shi GQ (2010) *Acs Nano* 4:1963–1970
33. Basavaraja C, Kim WJ, Kim YD, Huh DS (2011) *Mater Lett* 65:3120–3123
34. Park S, Ruoff RS (2009) *Nat Nanotechnol* 4:217–224
35. Stankovich S, Piner RD, Chen XQ, Wu NQ, Nguyen ST, Ruoff RS (2006) *J Mater Chem* 16:155–158
36. Muszynski R, Seger B, Kamat PV (2008) *J Phys Chem C* 112:5263–5266
37. Zhao Y, Bai H, Hu Y, Li Y, Qu L, Zhang S, Shi G (2011) *J Mater Chem* 21:13978–13983
38. Yang X, Zhang X, Ma Y, Yi H, Wang Y, Chen J (2009) *J Mater Chem* 19:2710–2714
39. Basavaraja C, Pierson R, Vishnuvardhan TK, Huh DS (2008) *Eur Poly J* 44:1556–1566
40. Basavaraja C, Veeragouda Y, Lee K, Pierson R, Huh DS (2009) *J Polym Sci B Polym Phys* 47:36–45
41. Basavaraja C, Kim WJ, Kim DG, Huh DS (2011) *Mater Chem Phys* 129:787–793
42. Zhang Z, Wei Z, Zhang L, Wan M (2005) *Acta Mater* 53:1373–1379
43. Xu J, Hu J, Quan B, Wei Z (2009) *Macromol Rapid Commun* 30:936–940
44. Huang J, Li Q, Sun D, Lu Y, Su Y, Yang X, Wang H, Wang Y, Shao W, He N, Hong J, Chen C (2007) *Nanotechnology* 18:105104–105113
45. Jie Huang, Meixiang WJ (1999) *Polym Sci A Polym Chem* 37:151–157
46. Huang J, Wan M (1999) *J Polym Sci A Polym Chem* 37:151–157
47. Asturias GE, MacDiarmid AG, McCall PR, Epstein AJ (1989) *Synth Met* 29:E157–E162
48. Eda G, Chhowalla M (2009) *Nano Lett* 9(2):814–818
49. Mallick K, Witcomb M, Scurrill M (2006) *Eur Phys J E* 20:347–353
50. Orendorff CJ, Sau TK, Murphy C (2006) *J Small* 2:636–639
51. Zhao X, Zhang Q, Chen D, Lu P (2010) *Macromolecules* 43(5):2357–2363
52. Joint Committee on Powder Diffraction Standards, Diffraction data file: JCPDS International Center for Diffraction Data: Swarthmore, PA 1991
53. Leff DV, Brandt L, Heath JR (1996) *Langmuir* 12:4723–4730
54. Zhang Z, Wei Z, Wan M (2002) *Macromolecules* 35:5937–5942
55. Wang LL, Tay BK, See KY, Sun Z, Tan LK, Lua D (2009) *Carbon* 47:1905–1910
56. Makeiff DA, Huber T (2006) *Synth Met* 156:497–505
57. Basavaraja C, Jo EA, Kim BS, Huh DS (2011) *Polym Compos* 32:438–444